JACS
JOURNAL OF THE AMERICAN CHEMICAL SOCIETY
Communication
pubs.acs.org/JACS

Photoelectrochemical Water Oxidation with Photosystem II Integrated in a Mesoporous Indium–Tin Oxide Electrode

Masaru Kato,[†] Tanai Cardona,[§] A. William Rutherford,[‡,§] and Erwin Reisner*[,†]

[†]Department of Chemistry, University of Cambridge, Lensfield Road, Cambridge CB2 1EW, U.K.
[‡]Division of Molecular Biosciences, Imperial College London, London SW7 2AZ, U.K.
[§]Institut de Biologie et Technologies de Saclay, URA 2096 CNRS, CEA Saclay, 91191 Gif-surYvette, France

Supporting Information

ABSTRACT: We report on a hybrid photoanode for water oxidation consisting of a cyanobacterial photosystem II (PSII) from *Thermosynechococcus elongatus* on a mesoporous indium–tin oxide (*meso*ITO) electrode. The three-dimensional metal oxide environment allows for high protein coverage (26 times an ideal monolayer coverage) and direct (mediator-free) electron transfer from PSII to *meso*ITO. The oxidation of water occurs with 1.6 ± 0.3 μA cm^{-2} and a corresponding turnover frequency of approximately 0.18 ± 0.04 (mol O_2) (mol PSII)$^{-1}$ s^{-1} during red light irradiation. Mechanistic studies are consistent with interfacial electron transfer occurring not only from the terminal quinone Q_B, but also from the quinone Q_A through an unnatural electron transfer pathway to the ITO surface.

Sunlight provides us with an effectively inexhaustible source of renewable energy and natural photosynthesis is an inspiration in the development of solar energy conversion systems.[1] The photolysis of water into H_2 and O_2 represents a sustainable route for the production of the energy vector, H_2.[2] Key requirements for this process to work are economical catalysts for proton reduction and water oxidation and their integration within a photovoltaic system for light harvesting and charge separation. The water oxidation reaction is often referred to as the bottleneck in water splitting, because of the inherent difficulty of catalyzing the overall four-electron/four-proton process.[3] Small one- or two-electron oxidation steps result in energetically unfavorable intermediates, for example, a hydroxyl radical (·OH).[4] Notable systems for the oxidation of water include cobalt-phosphate deposited on an indium–tin oxide (ITO) electrode,[5] and polyoxymetalates in the presence of a chemical oxidant.[6] A mononuclear pincer-type ruthenium based catalyst was reported to promote light-induced oxygen and consecutive thermal H_2 evolution.[7]

Despite the progress with such systems, Nature's water oxidizing enzyme photosystem II (PSII) sets a benchmark in terms of O_2 evolution rate under ambient conditions for the development of synthetic catalysts. Protein film voltammetry of PSII was reported previously on pyrolytic graphite disc electrodes, but photocatalytic O_2 evolution was not studied.[8] PSII was also utilized for photoelectrochemical water oxidation on noble metal electrodes, for example, Au and Pt.[9,10] However, the immobilization of PSII on these noble metal surfaces required modification of the metal surface with Os(II) redox polymers[9] or self-assembled thiolate-monolayers with terminal Ni(II)–nitrilotriacetic acid complexes.[10] Furthermore, such noble metal materials are also unsustainable, their flat and hydrophobic surface area prevents high protein loading and they absorb visible light, which complicates their application in photochemical devices.

In this communication, a hybrid photoanode consisting of the combination of a biological catalyst and a three-dimensional, biocompatible, solid-state material for water oxidation is presented. The catalyst, PSII isolated from the thermophilic cyanobacterium *Thermosynechococcus elongatus*, was integrated in a mesoporous ITO (*meso*ITO) electrode. The transmembrane protein complex PSII contains a highly sophisticated machinery for light absorption, charge separation, and water oxidation catalysis (Figure 1A). It provides the best means available for the oxidation of water in terms of catalytic rate and, therefore, provides a reference point for synthetic systems. *Meso*ITO is an excellent and emerging electrode material,[11] because it allows for high enzyme catalyst loading, high electrical conductivity, and an optical transparency as required for photoelectrochemical experiments.

*Meso*ITO was prepared on a surface area of 0.25 cm^2 by annealing ITO nanoparticles (<50 nm diameter) on ITO-coated glass slides at 450 °C. The resulting *meso*ITO films have a sheet resistance of 8.4 kΩ sq^{-1}, a thickness of approximately 3 μm, and a pore diameter up to 100 nm (for SEM images see Figure S1). Thus, they are well suited to incorporate *T. elongatus* PSII with its dimensions of approximately 11 × 11 × 21 nm.[16] Then, PSII was adsorbed on the *meso*ITO surface by putting a drop of PSII (1 μL of a 3.2 mg Chl mL^{-1} solution) on the electrode surface in the dark. After 1 h, the PSII-modified *meso*ITO electrode was immersed in the electrolyte solution for photoelectrochemical experiments.

Photocurrents were recorded with a PSII-modified *meso*ITO electrode at +0.5 V vs NHE under red light irradiation (635 nm, 8 mW cm^{-2}) at pH 6.5 and 25 °C. Typical photocurrent responses are summarized in Table 1 and Figure 1B with three cycles of a dark period followed by irradiation for 30 s each. Control experiments without PSII and with [Mn_4Ca]-cluster depleted PSII (removed by NH_2OH treatment) resulted in no photocurrent response. Thus, removal of the catalytic center for

Received: February 14, 2012
Published: May 1, 2012

 © 2012 American Chemical Society dx.doi.org/10.1021/ja301488d | *J. Am. Chem. Soc.* 2012, 134, 8332–8335

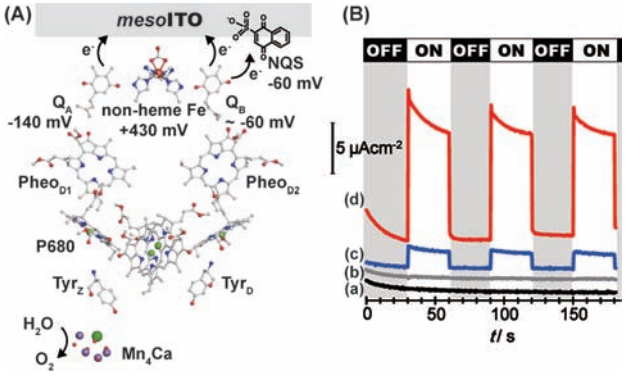

Figure 1. (A) Schematic representation of the arrangement of cofactors involved in an electron transfer chain in PSII and the redox potentials of Q_A,[12] Q_B,[12] the non-heme iron,[13] and NQS.[14] The arrangement of cofactors is depicted according to a recently published 1.9 Å crystal structure of PSII (pdb reference 3ARC).[15] (B) Representative photocurrent response of unmodified *meso*ITO (a, black trace), [Mn_4Ca]-cluster depleted-PSII-*meso*ITO (b, gray trace), PSII-*meso*ITO (c, blue trace), and PSII-*meso*ITO with 1 mM NQS (d, red trace). A bias potential of +0.5 V vs NHE was applied at 25 °C. A buffered solution containing 50 mM KCl, 15 mM $CaCl_2$, 15 mM $MgCl_2$, and 40 mM MES was used at pH 6.5. Dark (gray) and illumination (white) cycles (635 nm, 8 mW cm^{-1}) are shown.

Table 1. Summary of Photoresponse of PSII-*meso*ITO[a]

hybrid system	i/μA cm^{-2}[b]	TOF/(mol O_2) (mol PSII)$^{-1}$ s^{-1}[c]
$PSII_{[Mn4Ca]\text{-depleted}}$	—	—
PSII	1.6 ± 0.3	0.18 ± 0.04
PSII (45 °C)	2.2 ± 0.5[d]	0.22 ± 0.04[d]
PSII + NQS	12 ± 1	1.4 ± 0.1
PSII + DCBQ	22 ± 2	3.2 ± 0.4
PSII + DCMU	0.5 ± 0.1	0.05 ± 0.02

[a]Measurements were recorded with a bias potential of +0.5 V vs. NHE in an electrolyte solution at pH 6.5 and 25 °C (unless otherwise noted). [b]Based on initial photocurrent densities. [c]Turnover frequencies (TOFs) were calculated based on photocurrents obtained during 30 s red light irradiation (635 nm, 8 mW cm^{-2}) with four electrons per O_2 molecule. [d]Recorded at 45 °C.

water oxidation resulted in the expected lack of photocurrent response of PSII on *meso*ITO. Functional PSII with intact [Mn_4Ca]-cluster on *meso*ITO electrodes respond in less than 0.1 s to light exposure and a photocurrent of 1.6 ± 0.3 μA cm^{-2} is obtained (Table 1). Here, direct electronic coupling between PSII and the *meso*ITO surface is observed (note that no soluble redox mediator is present in solution), allowing for photocatalytic water oxidation with the described hybrid construct. Despite good stability in the dark, our hybrid electrode photodegrades with a half-life time of 4 to 5 min under continuous red light illumination (Figure S2).

We also explored the photoactivity of PSII-*meso*ITO at 45 °C, because increased O_2 evolution rates were previously reported for the thermophilic *T. elongatus* PSII.[17] In agreement, we observed an enhanced photoresponse of 2.2 ± 0.5 μA cm^{-2} at 45 °C (Table 1), but with increased photodegradation of the photoanode (Figure S3).

We also recorded photocurrents of PSII-modified *meso*ITO using different wavelengths (510, 535, 595, and 635 nm) with the same light intensity (2 mW cm^{-2}) at 25 °C. The action spectrum, that is photocurrent plotted as a function of wavelengths, reflects the absorbance profile of PSII: a minimum absorption in the green region of the solar spectrum and a maximum in the cyan and red region (Figure S4).

The following mechanism is proposed for the PSII-*meso*ITO electrode (Figure 1A). Excitation of the primary electron donor P680 results in donation of an electron to $Pheo_{D1}$ and a hole to Tyr_Z. The latter removes electrons from the [Mn_4Ca]-cluster, and upon multiple photochemical turnovers, water oxidation occurs forming O_2. The $Pheo_{D1}$ anion radical donates an electron to Q_A and the electron can then be transferred to Q_B. From the structure of PSII, direct interfacial electron transfer is only possible if electrons are delivered to the *meso*ITO surface from the quinones Q_A and Q_B in PSII.

PSII film photocurrent measurements were also performed in the presence of a soluble redox mediator (Figure 1B and Table 1), where electrons are collected by the mediator at PSII and delivered to *meso*ITO. Potassium 1,4-naphthoquinone-2-sulfonate (NQS) was selected as the mediator for the following reasons: it has a reduction potential comparable to the most recent estimate for Q_B[12] ($^{NQS}E_m$ = −60 mV vs NHE[14]) to minimize energy loss, and the sulfonate group provides a negatively charged affinity site for the positively charged ITO. This electrostatic interaction supports a high local concentration of NQS at the electrode surface. As expected, the presence of NQS (1 mM) enhanced the photoelectrochemical response and an initial photocurrent of 12 ± 1 μA cm^{-2} was obtained with the PSII-*meso*ITO electrode under red light illumination. We also used 2,6-dichloro-1,4-benzoquinone (DCBQ) as an electron mediator and we observed a photocurrent of 22 ± 2 μA cm^{-2} (Table 1). The enhanced photoresponse agrees with the increased driving force for the reduction of DCBQ ($^{DCBQ}E_m$ = +21 mV vs NHE)[18] compared to NQS. In principle most, if not all PSII can communicate via the mediators NQS or DCBQ with ITO under these conditions, whereas only PSII in the correct orientation and conformation can transfer electrons to ITO in the mediator-free system.

The photon-to-current quantum yield of our hybrid electrode was dependent on the light intensity and increased from approximately 0.04 to 0.3% when decreasing the red light intensity from 10 to 1 mW cm^{-2} (635 nm, +0.5 V vs NHE, in presence of 1 mM of NQS; Figure S5).

Potential electron donor sites in PSII are Q_A, the non-heme iron, and Q_B, which are approximately 10 Å away from the protein surface. Thus, electron transfer to *meso*ITO might in principle occur not only from the terminal electron acceptor, Q_B, but also from the non-heme ferrous ion and Q_A. The Fe^{II} is located between Q_A and Q_B and is coordinated by four histidine residues and a bidentate hydrogencarbonate ligand (Figure 1A). In redox terms, however, the ferrous ion is unlikely to play an important direct role, because we observed photocurrents down to a minimum bias potential of +0.2 V vs NHE, well below the midpoint potential (E_m) of the iron (+0.43 V vs NHE[13]).

PSII was reported to deliver electrons from Q_A to ferricyanide,[17] to cytochrome *c*,[19] and to a synthetic cationic Co^{III} complex[20] in the presence of the Q_B inhibitor 3′-(3,4-dichlorophenyl)-1,1′-dimethylurea (DCMU). These observations indicate an electron transfer pathway from Q_A to an external electron acceptor site. When we added the herbicide DCMU (1 mM) to the PSII-*meso*ITO system to inhibit Q_B and block electron transfer from Q_A to Q_B, a significant residual level of photocurrent remained (0.5 ± 0.1 μA cm^{-2}). This is taken as an indication of direct electron transfer from Q_A to the *meso*ITO (Table 1, Figure S6). We conclude from this

dx.doi.org/10.1021/ja301488d | J. Am. Chem. Soc. 2012, 134, 8332−8335

experiment that $Q_B \rightarrow$ ITO electron transfer dominates in our hybrid photoanode, but electron injection into ITO is also possible through Q_A. Electron capture at Q_A level allows us to avoid the slow Q_B diffusion kinetics and might give access to faster electron transfer and better energetics, all important aspects for the efficiency of future versions of this system.

The amount of PSII on *meso*ITO was determined in order to calculate PSII coverage and turnover rates with our PSII-modified photoanode. The PSII-ITO nanoparticles were scratched off the electrode after photoelectrochemical measurements and the enzyme-ITO particles were suspended in MeOH (1 mL) to solubilize the chlorophylls in the methanolic solution, centrifuged, and removed by filtration. Electronic absorption spectrophotometry allowed the amount of chlorophyll *a* in the methanolic solution to be calculated as 0.17 ± 0.03 nmol mL^{-1} (see Supporting Information). This corresponds to a PSII density on *meso*ITO of approximately 19 pmol PSII cm^{-2} with 35 chlorophyll *a* molecules per PSII and 0.25 cm^2 surface areas. This high surface coverage is about 26 times higher than for a monolayer coverage of PSII on an ideal two-dimensional surface.[21] Thus, the three-dimensional ITO surface architecture allows for a densely packed PSII film, which is approximately 51 times higher than the PSII coverage on a previously reported Ni(II)−nitrilotriacetic acid−Au surface (~0.37 pmol PSII cm^{-2}).[10a]

A turnover frequency (TOF) of 0.18 (mol O_2) (mol PSII)$^{-1}$ s^{-1} was obtained for PSII-*meso*ITO and 1.4 (mol O_2) (mol PSII)$^{-1}$ s^{-1} for PSII-*meso*ITO in the presence of NQS assuming all PSII is photoactive in this system (Table 1). The TOF of our light-induced oxygen evolution assembly compares favorably with synthetic electrochemical systems. A TOF up to 0.075 s^{-1} at +1.2 V vs NHE was reported for the precatalyst $[Mn_4O_4(MeOPh_2PO_2)]$ in a Nafion film on a glassy carbon electrode,[22] which converts in situ to catalytically active Mn(III/IV)−oxide nanoparticles.[18] A cobalt-phosphate water oxidation electrocatalyst on ITO was reported to have structural similarity to the $[Mn_4Ca]$-cluster in PSII,[5] and a current density of >1 mA cm^{-2} was reported at room temperature,[5] which corresponds to a TOF of more than 0.002 s^{-1} per Co center.[23,24]

In summary, we report on a water-oxidizing photoanode consisting of PSII integrated in a *meso*ITO electrode. The three-dimensional and hydrophilic metal oxide surface supports photoactive and stable enzyme films and promotes high protein loadings. Its optical transparency allows for the development of optically driven bioelectrochemical devices. Photoexcitation of PSII results in water oxidation at the $[Mn_4Ca]$-cluster and electron flow to the *meso*ITO electrode. Interfacial electron transfer occurs directly with a minimum applied bias potential of +0.2 V vs NHE during red light illumination via two competing pathways, Q_A and Q_B, to the ITO surface. Mediator-free coupling is important, because mediators are undesirable from a kinetic and thermodynamic perspective: rates are diffusion limited at best (prohibiting tight electronic coupling) and electrons are only delivered with the reduction potential of the mediator (thereby generating heat loss in the system). The direct coupling of the photosynthetic machinery of PSII on *meso*ITO sets a benchmark for synthetic electro- and photocatalytic water oxidation catalysts on a per active site basis. The reported hybrid construct might also allow us to determine the accurate redox potentials of the cofactors in PSII by direct protein film voltammetry and work is in progress to combine the reported PSII-*meso*ITO electrode with a H_2 evolving photocathode for overall solar water splitting.

■ ASSOCIATED CONTENT

Supporting Information

Experimental details, SEM images of *meso*ITO, and figures on various photoelectrochemical measurements. This material is available free of charge via the Internet at http://pubs.acs.org.

■ AUTHOR INFORMATION

Corresponding Author

*reisner@ch.cam.ac.uk

Notes

The authors declare no competing financial interest.

■ ACKNOWLEDGMENTS

The Engineering and Physical Sciences Research Council (Career Acceleration Fellowship EP/H00338X and Strategic Fund to E.R.), the Royal Society for a Research Grant (to E.R.), the Japan Society for the Promotion of Science (Grant-in-Aid 21007915 to M.K.), EU (SOLARH2 project no 212508 to A.W.R.), the ANR (PROTOCOLE to A.W.R.) and the University of Cambridge supported this work. T.C. is supported by a Eurotalents grant from the EU and A.W.R. is the recipient of the Wolfson Merit Award of the Royal Society. We are also grateful to Mr. Dirk Mersch for helping in preparing SEM images of *meso*ITO, Dr. Chia-Yu Lin for measuring the sheet resistance of *meso*ITO, and Dr. Andrea Fantuzzi, Dr. Benedict Lassalle, Dr. Paolo Bombelli, and Dr. Alistair J. McCormick for fruitful discussions.

■ REFERENCES

(1) Blankenship, R. E.; Tiede, D. M.; Barber, J.; Brudvig, G. W.; Fleming, G.; Ghirardi, M.; Gunner, M. R.; Junge, W.; Kramer, D. M.; Melis, A.; Moore, T. A.; Moser, C. C.; Nocera, D. G.; Nozik, A. J.; Ort, D. R.; Parson, W. W.; Prince, R. C.; Sayre, R. T. *Science* **2011**, *332*, 805−809.

(2) Reece, S. Y.; Hamel, J. A.; Sung, K.; Jarvi, T. D.; Esswein, A. J.; Pijpers, J. J. H.; Nocera, D. G. *Science* **2011**, *334*, 645−648.

(3) Hurst, J. K. *Science* **2010**, *328*, 315−316.

(4) Meyer, T. J. *Nature* **2008**, *451*, 778−779.

(5) Kanan, M. W.; Nocera, D. G. *Science* **2008**, *321*, 1072−1075.

(6) Yin, Q.; Tan, J. M.; Besson, C.; Geletii, Y. V.; Musaev, D. G.; Kuznetsov, A. E.; Luo, Z.; Hardcastle, K. I.; Hill, C. L. *Science* **2010**, *328*, 342−345.

(7) Kohl, S. W.; Weiner, L.; Schwartsburd, L.; Konstantinovski, L.; Shimon, L. J. W.; Ben-David, Y.; Iron, M. A.; Milstein, D. *Science* **2009**, *324*, 74−77.

(8) Alcantara, K.; Munge, B.; Pendon, Z.; Frank, H. A.; Rusling, J. F. *J. Am. Chem. Soc.* **2006**, *128*, 14930−14937.

(9) Badura, A.; Guschin, D.; Esper, B.; Kothe, T.; Neugebauer, S.; Schuhmann, W.; Rögner, M. *Electroanalysis* **2008**, *20*, 1043−1047.

(10) (a) Badura, A.; Esper, B.; Ataka, K.; Grunwald, C.; Wöll, C.; Kuhlmann, J.; Heberle, J.; Rögner, M. *Photochem. Photobiol.* **2006**, *82*, 1385−1390. (b) Terasaki, N.; Iwai, M.; Yamamoto, N.; Hiraga, T.; Yamada, S.; Inoue, Y. *Thin Solid Films* **2008**, *516*, 2553−2557.

(11) Liu, F.; Cardolaccia, T.; Hornstein, B. J.; Schoonover, J. R.; Meyer, T. J. *J. Am. Chem. Soc.* **2007**, *129*, 2446−2447.

(12) Shibamoto, T.; Kato, Y.; Sugiura, M.; Watanabe, T. *Biochemistry* **2009**, *48*, 10682−10684.

(13) Diner, B. A.; Petrouleas, V. *Biochim. Biophys. Acta* **1987**, *895*, 107−125.

(14) Ilan, Y. A.; Czapski, G.; Meisel, D. *Biochim. Biophys. Acta* **1976**, *430*, 209−224.

(15) Umena, Y.; Kawakami, K.; Shen, J.-R.; Kamiya, N. *Nature* **2011**, *473*, 55−60.
(16) Ferreira, K. N.; Iverson, T. M.; Maghlaoui, K.; Barber, J.; Iwata, S. *Science* **2004**, *303*, 1831−1838.
(17) Sugiura, M.; Inoue, Y. *Plant Cell Physiol.* **1999**, *40*, 1219−1231.
(18) Zhu, X. Q.; Wang, C. H. *J. Org. Chem.* **2010**, *75*, 5037−5047.
(19) Larom, S.; Salama, F.; Schuster, G.; Adir, N. *Proc. Natl. Acad. Sci. U.S.A.* **2010**, *107*, 9650−9655.
(20) Ulas, G.; Brudvig, G. W. *J. Am. Chem. Soc.* **2011**, *133*, 13260−13263.
(21) Vittadello, M.; Gorbunov, M. Y.; Mastrogiovanni, D. T.; Wielunski, L. S.; Garfunkel, E. L.; Guerrero, F.; Kirilovsky, D.; Sugiura, M.; Rutherford, A. W.; Safari, A.; Falkowski, P. G. *ChemSusChem* **2010**, *3*, 471−475.
(22) Brimblecombe, R.; Kolling, D. R. J.; Bond, A. M.; Dismukes, G. C.; Swiegers, G. F.; Spiccia, L. *Inorg. Chem.* **2009**, *48*, 7269−7279.
(23) Shevchenko, D.; Anderlund, M. F.; Thapper, A.; Styring, S. *Energy Environ. Sci.* **2011**, *4*, 1284−1287.
(24) Surendranath, Y.; Kanan, M. W.; Nocera, D. G. *J. Am. Chem. Soc.* **2010**, *132*, 16501−16509.